GESTURE RECOGNITION FROM MAGNETIC FIELD MEASUREMENTS USING A BANK OF LINEAR STATE SPACE MODELS AND LOCAL LIKELIHOOD FILTERING

Nour Zalmai, Christian Kaeslin, Lukas Bruderer, Sarah Neff, and Hans-Andrea Loeliger

ETH Zurich
Dept. of Information Technology & Electrical Engineering
{zalmai, bruderer, sneff, loeliger}@isi.ee.ethz.ch, christian.kaeslin@alumni.ethz.ch

ABSTRACT

Detecting and inferring the trajectory of a moving magnet from magnetic field measurements is a challenge due to a wide range of time scales and amplitudes of the recorded signals and limited computational power of devices embedding a magnetometer. In this paper, we model the magnetic field measurements using a bank of autonomous linear state space models and provide an efficient algorithm based on local likelihood filtering for reliably detecting and inferring the gesture causing the magnetic field variations.

Index Terms— Gesture recognition, linear state space models, local likelihood filtering, magnetometer

1. INTRODUCTION

Contemporary smartphones embed a magnetometer that measures the magnetic field in three dimensions. Sweeping over the phone with a magnet induces magnetic field variations which are measured by the magnetometer. Given these 3-channel signals (e.g., as plotted in Figure 2), we want to design a real-time smartphone application which infers the movement of the magnet. Such gestures can be used to give commands to the phone without any contact and possibly with obstructing objects.

A current approach [1] consists in defining a finite set of movements and extracting a feature vector from the measurements. Then, a multi-layer perceptron assigns each feature vector to one of the predefined movements. This type of methods considerably limits the number of possible gestures and generally requires a good SNR (i.e., a strong magnet).

In the context of tracking a general target modeled as a magnetic dipole using magnetic field measurements, popular approaches [2–7] consist in using recursive Bayesian estimation methods (e.g., a particle filter or an extended Kalman filter (EKF)) for tracking the position, velocity, and magnetic moment of the target. Such algorithms are able to track arbitrary trajectories. However these approaches require two magnetometers and considerable computational power. Besides, the reported results were obtained with much lower noise than what is encountered with smartphone sensors.

Another approach consists in extracting and handling information from the dipole equation. Such information is included in the EKF equations [5,6] and is also exploited to validate a physical model [7]. In [8], Otnes uses a finite-impulse response (FIR) matched filter derived from the dipole equation to detect straight-line movements. Unfortunately, the signals are processed blockwise (not computationally efficient) and a large detection delay per time-scale is reported. As a result this method is not suitable for real-time application.

In this paper, we propose an efficient algorithm for detecting and inferring uniform straight-line movements of a magnet with only one magnetometer. Since strong magnets are potentially harmful for surrounding magnetic devices such as hard drives or stripe cards, the recognition should also work in a low SNR regime with weak magnets that are ubiquitous in everyday life (e.g., standard earphones). Furthermore the algorithm is intended to be implemented on a smartphone and to run in real-time. Therefore a low complexity (linear if possible) and a short detection delay are of main importance.

After deriving useful properties of the magnetic field induced by a moving magnet in Section 2, this paper describes an algorithm which meets all the above requirements. We model the magnetic field measurements with a bank of low-order state space models where the observation matrix contains the information of the movement (Section 3). Efficient recursions are derived to compute localized squared errors and a method is described for estimating the gesture parameters (Section 4). The algorithm is tested on simulated and recorded data (Section 5) and demonstrates promising results.

2. MAGNETIC FIELD CHARACTERIZATION

We use the coordinate system of the magnetometer. Let $\mathbf{r}_k \in \mathbb{R}^3$ be the magnet position at time index $k \in \mathbb{Z}$. The magnetic field vector $\mathbf{B}_k$ induced by a dipole at position $\mathbf{r}_k$ is

$$\mathbf{B}_k = \frac{\mu_0}{4\pi} \left(\frac{3 \langle \mathbf{m}, \mathbf{r}_k \rangle \, \mathbf{r}_k}{\|\mathbf{r}_k\|^5} - \frac{\mathbf{m}}{\|\mathbf{r}_k\|^3} \right), \tag{1}$$

where $\mathbf{m} \in \mathbb{R}^3$ is the magnetic moment of the magnet and $\mu_0 = 4\pi \times 10^{-7}\,\mathrm{N/A^2}$ is the vacuum permeability.

We consider a discrete uniform rectilinear movement $\mathbf{r}_k \in \mathbb{R}^3$, $k \in \mathbb{Z}$, which starts and ends far away from the magnetometer (i.e., $\|\mathbf{r}_k\| \to +\infty$ as $k \to \pm\infty$). Without loss of generality we assume that the minimum distance r is reached at $k = 0$ and thus, such movement can be parametrized as

$$\mathbf{r}_k = r\mathbf{d}_r + kv\mathbf{d}_v = r(\mathbf{d}_r + \frac{k}{\tau}\mathbf{d}_v), \tag{2}$$

where $r \in \mathbb{R}_+$ is the minimum distance to the magnetometer, $\mathbf{d}_r \in \mathbb{R}^3$ is the unit direction when achieving this minimum distance, $v \in \mathbb{R}_+$ is the constant per sample speed, $\mathbf{d}_v \in \mathbb{R}^3$ is the unit direction of the movement, and $\tau = \frac{r}{v}$ is the time-scale parameter. Note that $\langle \mathbf{d}_r, \mathbf{d}_v \rangle = 0$ due to the minimum distance characterization of $\mathbf{d}_r$.

Let $(\mathbf{e}_x, \mathbf{e}_y, \mathbf{e}_z)$ be the canonical basis of the magnetometer. A uniform straight-line movement can be reparametrized by $(r, R, \tau) \in \mathbb{R}_+ \times \mathcal{SO}_3(\mathbb{R}) \times \mathbb{R}_+$. Indeed, by ensuring that $R\mathbf{e}_x = \mathbf{d}_r$, $R\mathbf{e}_y = \mathbf{d}_v$, and $R\mathbf{e}_z = \mathbf{d}_r \times \mathbf{d}_v$, we get

$$\mathbf{r}_k = rR(\mathbf{e}_x + \frac{k}{\tau}\mathbf{e}_y). \tag{3}$$

Note that $\|\mathbf{r}_k\|^2 = r^2(1 + \left(\frac{k}{\tau}\right)^2)$ is independent of R.

The moment $\mathbf{m} = m\mathbf{d}_m$ ($m \in \mathbb{R}_+$ and $\|\mathbf{d}_m\| = 1$) of the magnet is considered independent of time (i.e., no rotation of the magnet during a movement). Furthermore we assume that $\mathbf{d}_m$ is orthogonal to the direction of the movement $\mathbf{d}_v$. Therefore there exists a unique $\phi \in]-\pi, \pi]$ such that

$$\mathbf{d}_m = \cos(\phi)R\mathbf{e}_x + \sin(\phi)R\mathbf{e}_z. \tag{4}$$

This last assumption is approximately satisfied if the magnet is held correctly. The inner product $\langle \mathbf{m}, \mathbf{r}_k \rangle$ simplifies into

$$\langle \mathbf{m}, \mathbf{r}_k \rangle = mr\cos(\phi) \tag{5}$$

and is now independent of time.

Finally, plugging (3), (4), and (5) into (1) and writing it in the matrix form in the basis $(\mathbf{e}_x, \mathbf{e}_y, \mathbf{e}_z)$, we get

$$\mathbf{B}_k = \lambda R D_\phi F \mathbf{G}_k \tag{6}$$

$$\mathbf{G}_k = \frac{1}{\left(1 + \left(\frac{k}{\tau}\right)^2\right)^{\frac{5}{2}}} \begin{bmatrix} 1 - \frac{1}{2}\left(\frac{k}{\tau}\right)^2 \\ \frac{k}{\tau} \\ 1 + \left(\frac{k}{\tau}\right)^2 \end{bmatrix} \tag{7}$$

with $D_\phi = \begin{bmatrix} \cos\phi & 0 & 0 \\ 0 & \cos\phi & 0 \\ 0 & 0 & \sin\phi \end{bmatrix}$, $F = \begin{bmatrix} 2 & 0 & 0 \\ 0 & 3 & 0 \\ 0 & 0 & -1 \end{bmatrix}$, and $\lambda = \frac{\mu_0 m}{4\pi r^3}$. As a movement starts and ends far away from the magnetometer, $\mathbf{B}_k \to 0$ as $k \to \pm\infty$.

The parameter τ essentially accounts for the time-scale (i.e, the signals are roughly supported on $[-8\tau, 8\tau]$), r is the closest distance to the magnetometer, R contains the direction of the gesture, and ϕ pinpoints the direction of the moment. In order to uniquely define $\mathbf{r}_k$ from $\mathbf{B}_k$ we must restrict ϕ to the interval $]-\frac{\pi}{2}, \frac{\pi}{2}[$, which constrains the way we hold the magnet when performing a movement.

3. MODELING MAGNETIC FIELD SIGNALS

Consider for a moment continuous-time signals rather than discrete-time signals (replace $k \in \mathbb{Z}$ by $t \in \mathbb{R}$).

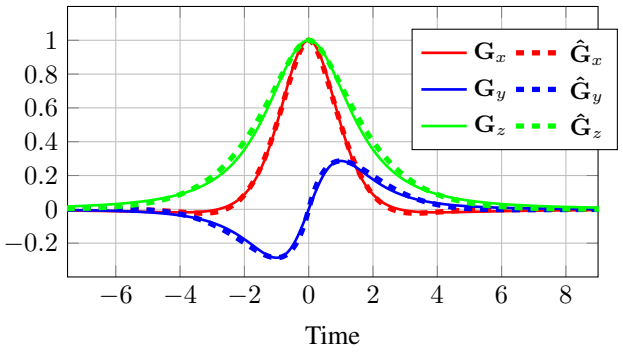

Fig. 1. Shape of the components of $\mathbf{G}_k$ and $\hat{\mathbf{G}}_k$ for a given τ

Looking at Figure 1, it seems that modeling each component of $\mathbf{G}(t)$ using a 2nd-order linear state space model is good enough for our gesture recognition purposes. Taking into consideration the symmetry properties and the scaling of the components of $\mathbf{G}(t)$, the estimated 3D-signal has the form

$$\hat{\mathbf{G}}(t) = \begin{bmatrix} e^{-\alpha_x|\frac{t}{\tau}|}\frac{\cos(\omega_x|\frac{t}{\tau}|+\Phi_x)}{\cos\Phi_x} \\ Ke^{-\alpha_y|\frac{t}{\tau}|}\sin(\omega_y\frac{t}{\tau}) \\ e^{-\alpha_z|\frac{t}{\tau}|}\frac{\cos(\omega_z|\frac{t}{\tau}|+\Phi_z)}{\cos\Phi_z} \end{bmatrix}. \tag{8}$$

The parameters α_x, ω_x, Φ_x, K, α_y, ω_y, α_z, ω_z, and Φ_z must not depend on τ and can be chosen to minimize

$$\int_{-\infty}^{+\infty} \|\mathbf{G}(t) - \hat{\mathbf{G}}(t)\|^2 \, \mathrm{d}t. \tag{9}$$

Unfortunately, analytical expressions are not available. Therefore we determine some of the parameters by imposing meaningful properties of $\mathbf{G}(t)$ to $\hat{\mathbf{G}}(t)$:

1. first derivatives of $G_x(t)$ and $G_z(t)$ both zero at $t = 0$
2. position and value of extrema of $G_y(t)$

which translates into

$$\Phi_a = -\arctan\left(\frac{\alpha_a}{\omega_a}\right) + \pi, \forall a \in \{x, z\} \tag{10}$$

$$\omega_y = 2\arctan(r_y) \tag{11}$$

$$K = \left(\frac{4}{5}\right)^{\frac{5}{2}} \frac{1}{2r_y}\sqrt{1 + r_y^2}\, e^{\frac{1}{r_y}\arctan r_y} \tag{12}$$

with $r_y = \frac{\omega_y}{\alpha_y}$ (similar definition for r_x and r_z, respectively).

The remaining parameters α_x, ω_x, r_y, α_z, and ω_z can be found by a grid-search minimization of the expression in (9). The parameters we obtained are $r_x = 0.83$, $\omega_x = 1.884$, $r_y = 0.64$, $\omega_y = 1.139$, $r_z = 0.12$, $\omega_z = 0.239$. In Figure 1, we observe $\mathbf{G}(t)$ and its estimate $\hat{\mathbf{G}}(t)$.

Using the following quantities

$$R_2(\omega) = \begin{bmatrix} \cos\omega & -\sin\omega \\ \sin\omega & \cos\omega \end{bmatrix} \tag{13}$$

$$A_a^{\mathrm{p}} = e^{\frac{\alpha_a}{\tau}} R_2(\frac{\omega_a}{\tau}), \forall a \in \{x, y, z\} \tag{14}$$

$$A_a^{\mathrm{f}} = e^{-\frac{\alpha_a}{\tau}} R_2(-\frac{\omega_a}{\tau}), \forall a \in \{x, z\} \tag{15}$$

$$A_y^{\mathrm{f}} = e^{-\frac{\alpha_y}{\tau}} R_2(\frac{\omega_y}{\tau}) \tag{16}$$

$$A_{\mathrm{p}} = \mathrm{Diag}(A_x^{\mathrm{p}}, A_y^{\mathrm{p}}, A_z^{\mathrm{p}}) \in \mathbb{R}^{6\times 6} \tag{17}$$

$$A_{\mathrm{f}} = \mathrm{Diag}(A_x^{\mathrm{f}}, A_y^{\mathrm{f}}, A_z^{\mathrm{f}}) \in \mathbb{R}^{6\times 6} \tag{18}$$

$$\mathbf{s} = \begin{bmatrix} 1 & 0 & 1 & 0 & 1 & 0 \end{bmatrix}^{\mathsf{T}} \tag{19}$$

$$\tilde{C} = \begin{bmatrix} 1 & \tan\Phi_x & 0 & 0 & 0 & 0 \\ 0 & 0 & 0 & K & 0 & 0 \\ 0 & 0 & 0 & 0 & 1 & \tan\Phi_z \end{bmatrix} \tag{20}$$

we can generate $\hat{\mathbf{B}}_k$ with a 6^{th}-order linear state space model

$$\hat{\mathbf{B}}_k = \begin{cases} \lambda R D_\phi C A_{\mathrm{p}}^k \mathbf{s}\,, & k \leq 0 \\ \lambda R D_\phi C A_{\mathrm{f}}^k \mathbf{s}\,, & k > 0 \end{cases}, \tag{21}$$

where $C = F\tilde{C}$. As the state transition matrices A_{p} and A_{f} depend on τ, we need one model per time scale.

4. DETECTING AND INFERRING GESTURES

Suppose we observe the noisy magnetic field measurements $\mathbf{y}_1, \ldots, \mathbf{y}_n \in \mathbb{R}^3$ and we want to test whether a gesture was made at time step $k = n - \delta$ for a fixed delay $\delta \in \mathbb{N}$. Since our algorithm will run in real-time (multiple gestures will be made) we localize the squared error with an exponential window of parameter $\gamma_\tau < 1$ (depending on τ only):

$$J_k(\lambda, R, \phi, \tau) = \sum_{i=1}^{k} \gamma_\tau^{|i-k|} \|\mathbf{y}_i - \lambda R D_\phi C A_{\mathrm{p}}^{i-k} \mathbf{s}\|^2 + \sum_{i=k+1}^{n} \gamma_\tau^{|i-k|} \|\mathbf{y}_i - \lambda R D_\phi C A_{\mathrm{f}}^{i-k} \mathbf{s}\|^2. \tag{22}$$

4.1. Efficient Computation of the Cost Function

Both terms in (22) can be efficiently computed using forward and backward recursions [9]. Indeed, expanding the first term of the cost leads to

$$\begin{aligned} &\sum_{i=1}^{k} \gamma_\tau^{|i-k|} \|\mathbf{y}_i - \lambda R D_\phi C A_{\mathrm{p}}^{i-k} \mathbf{s}\|^2 \\ &= \sum_{i=1}^{k} \gamma_\tau^{|i-k|} \|\mathbf{y}_i\|^2 - 2\lambda \operatorname{Tr}\left(R D_\phi C \sum_{i=1}^{k} \gamma_\tau^{|i-k|} A_{\mathrm{p}}^{i-k} \mathbf{s}\mathbf{y}_i^{\mathsf{T}} \right) \\ &\quad + \lambda^2 \operatorname{Tr}\left(D_\phi^2 C \sum_{i=1}^{k} \gamma_\tau^{|i-k|} A_{\mathrm{p}}^{i-k} \mathbf{s}\mathbf{s}^{\mathsf{T}} (A_{\mathrm{p}}^{i-k})^{\mathsf{T}} C^{\mathsf{T}} \right) \qquad (23) \\ &= \overrightarrow{\kappa}_k - 2\lambda \operatorname{Tr}\left(R D_\phi C \overrightarrow{\xi}_k \right) + \lambda^2 \operatorname{Tr}\left(D_\phi^2 C \overrightarrow{W}_k C^{\mathsf{T}} \right), \qquad (24) \end{aligned}$$

where $\operatorname{Tr}(M) = \sum_i M_{i,i}$, $\overrightarrow{\kappa}_k \in \mathbb{R}$, $\overrightarrow{\xi}_k \in \mathbb{R}^{6\times 3}$, and $\overrightarrow{W}_k \in \mathbb{R}^{6\times 6}$. In terms of these parameters, the forward recursion is

$$\overrightarrow{W}_k = \gamma_\tau A_{\mathrm{p}}^{-1} \overrightarrow{W}_{k-1} \left(A_{\mathrm{p}}^{-1}\right)^{\mathsf{T}} + \mathbf{s}\mathbf{s}^{\mathsf{T}} \tag{25}$$

$$\overrightarrow{\xi}_k = \gamma_\tau A_{\mathrm{p}}^{-1} \overrightarrow{\xi}_{k-1} + \mathbf{s}\mathbf{y}_k^{\mathsf{T}} \tag{26}$$

$$\overrightarrow{\kappa}_k = \gamma_\tau \overrightarrow{\kappa}_{k-1} + \|\mathbf{y}_k\|^2 \tag{27}$$

with the initializations $\overrightarrow{W}_0 = 0$, $\overrightarrow{\xi}_0 = 0$, and $\overrightarrow{\kappa}_0 = 0$.

The second term of the cost function can be parametrized in a same way, leading to the backward recursion

$$\overleftarrow{W}_k = \gamma_\tau \left(A_{\mathrm{f}} \overleftarrow{W}_{k+1} A_{\mathrm{f}}^{\mathsf{T}} + A_{\mathrm{f}} \mathbf{s}\mathbf{s}^{\mathsf{T}} A_{\mathrm{f}}^{\mathsf{T}} \right) \tag{28}$$

$$\overleftarrow{\xi}_k = \gamma_\tau \left(A_{\mathrm{f}} \overleftarrow{\xi}_{k+1} + A_{\mathrm{f}} \mathbf{s}\mathbf{y}_{k+1}^{\mathsf{T}} \right) \tag{29}$$

$$\overleftarrow{\kappa}_k = \gamma_\tau \left(\overleftarrow{\kappa}_{k+1} + \|\mathbf{y}_{k+1}\|^2 \right) \tag{30}$$

with the initializations $\overleftarrow{W}_n = 0$, $\overleftarrow{\xi}_n = 0$, and $\overleftarrow{\kappa}_n = 0$.

Finally, denoting $W_k = \overrightarrow{W}_k + \overleftarrow{W}_k$, $\xi_k = \overrightarrow{\xi}_k + \overleftarrow{\xi}_k$, $\kappa_k = \overrightarrow{\kappa}_k + \overleftarrow{\kappa}_k$, the cost function $J_k(\lambda, R, \phi, \tau)$ is

$$\kappa_k - 2\lambda \operatorname{Tr}\left(R D_\phi C \xi_k \right) + \lambda^2 \operatorname{Tr}\left(D_\phi^2 C W_k C^{\mathsf{T}} \right). \tag{31}$$

The backward messages introduce a fixed delay of $\delta = n - k$. Note that when a new observation $\mathbf{y}_{n+1}$ is available, a more efficient update for the backward messages is

$$\overleftarrow{W}_{k+1}^{(n+1)} = \overleftarrow{W}_k^{(n)} \tag{32}$$

$$\overleftarrow{\xi}_{k+1}^{(n+1)} = \gamma_\tau^{-1} A_{\mathrm{f}}^{-1} \overleftarrow{\xi}_k^{(n)} + \gamma_\tau^{\delta} A_{\mathrm{f}}^{\delta} \mathbf{s}\mathbf{y}_{n+1}^{\mathsf{T}} - \mathbf{s}\mathbf{y}_{k+1}^{\mathsf{T}} \tag{33}$$

$$\overleftarrow{\kappa}_{k+1}^{(n+1)} = \gamma_\tau^{-1} \overleftarrow{\kappa}_k^{(n)} + \gamma_\tau^{\delta} \|\mathbf{y}_{n+1}\|^2 - \|\mathbf{y}_{k+1}\|^2 \tag{34}$$

where $(\cdot)^{(n)}$ denotes the message when observing $\mathbf{y}_1, \ldots, \mathbf{y}_n$.

4.2. Minimizing the Cost Function

For a fixed time scale τ, we focus on minimizing J_k with respect to λ, R, and ϕ. Using short notations, we have

$$J(\lambda, R, \phi) = \kappa - 2\lambda \operatorname{Tr}\left(R D_\phi M \right) + \lambda^2 \operatorname{Tr}\left(D_\phi^2 W \right), \tag{35}$$

with $M, W \in \mathbb{R}^{3\times 3}$ and W a symmetric positive semi-definite matrix. We reparametrize the function such that

$$J(\beta, O, \eta) = \kappa - 2\beta \operatorname{Tr}\left(O L_\eta M \right) + \beta^2 \operatorname{Tr}\left(L_\eta^2 W \right), \tag{36}$$

with $\beta = \lambda \cos\phi \geq 0$, $\eta = |\tan\phi| \geq 0$, $L_\eta = \mathrm{Diag}(1, 1, \eta)$,

$$O = R \begin{bmatrix} 1 & 0 & 0 \\ 0 & 1 & 0 \\ 0 & 0 & \frac{\tan\phi}{|\tan\phi|} \end{bmatrix} \in \mathcal{O}_3(\mathbb{R}). \tag{37}$$

For a fixed η, using the SVD decomposition $L_\eta M = U_\eta \Sigma_\eta V_\eta^{\mathsf{T}}$, the optimum values are given by (Orthogonal Procrustes problem [10]) $\hat{O} = V_\eta U_\eta^{\mathsf{T}}$, $\hat{\beta} = \frac{\operatorname{Tr}(\Sigma_\eta)}{\operatorname{Tr}\left(L_\eta^2 W\right)}$, and

$$\min_{\beta, O} J(\beta, O, \eta) = \kappa - \frac{\operatorname{Tr}\left(\Sigma_\eta\right)^2}{\operatorname{Tr}\left(L_\eta^2 W\right)}. \tag{38}$$

Unfortunately, a joint minimization of the cost with respect to β, O, and η did not lead to a drastically more efficient search of the optimum parameters. Therefore a grid search (i.e., discretization of ϕ) is used

$$J_{\min} = \min_{i \in I} \min_{\beta, O} J(\beta, O, \eta_i), \tag{39}$$

where $I \subset \mathbb{N}$. The range of ϕ can be restricted to $[0, \frac{\pi}{2}[$. Indeed consider the two optimization problems for ϕ and $-\phi$. They share the same optimum $\hat{O} = V_\eta U_\eta^\mathsf{T}$ but the relation $\det \hat{O} = \pm 1$ (from Equation (37)) is valid only for one of the ϕ's, which induces a smaller cost for the incompatible ϕ. We know right away the best angle to choose between ϕ and $-\phi$.

4.3. Detection and Estimation

We define the local log-likelihood function [9]

$$\ln \breve{p}_k(y_1, \ldots, y_n; \lambda, R, \phi, \tau) = -\frac{1}{2} \ln(2\pi J_k(\lambda, R, \phi, \tau)) - \frac{1}{2}. \tag{40}$$

In order to detect a gesture at time step $k = n - \delta$, for a given time-scale τ, we use the hypothesis test

- $\mathcal{H}_0$: $\lambda = 0$
- $\mathcal{H}_1$: $\lambda > 0$, $R \in \mathcal{SO}_3(\mathbb{R})$, $\phi \in]-\frac{\pi}{2}, \frac{\pi}{2}[$

and the following log-likelihood ratio

$$\mathrm{LLR}_k^{(\tau)} = \ln \frac{\max\limits_{\lambda, R, \phi} \breve{p}_k(y_1, \ldots, y_n; \lambda, R, \phi, \tau)}{\breve{p}_k(y_1, \ldots, y_n; \lambda = 0, R, \phi, \tau)}, \tag{41}$$

where the maximization in the numerator is such that $\lambda \geq 0$, $R \in \mathcal{SO}_3(\mathbb{R})$, $\phi \in]-\frac{\pi}{2}, \frac{\pi}{2}[$. The denominator does not depend on R and ϕ due to $\lambda = 0$.

At time step k, let $\hat{\eta}^k$ be the optimum η in the discrete set $\{\eta_i, i \in I\}$, which can be found using (38) and (39). The approximate log-likelihood ratio at time scale τ is

$$\mathrm{LLR}_k^{(\tau)} = -\frac{1}{2} \ln \left(1 - \frac{\mathrm{Tr}\left(\Sigma_{\hat{\eta}^k}\right)^2}{\kappa_k \, \mathrm{Tr}\left(L_{\hat{\eta}^k}^2 C W_k C^\mathsf{T}\right)} \right). \tag{42}$$

In order to take into account several time scales, we discretize the parameter $\tau \in \{\tau_j, j \in J \subset \mathbb{N}\}$. Each τ has its own state space model and the final quantity we use is

$$\mathrm{LLR}_k = \max_{j \in J} \mathrm{LLR}_k^{(\tau_j)}. \tag{43}$$

If LLR_k is above a threshold ϵ and locally maximum then a gesture is detected and the estimated gesture parameters can be retrieved using the method described in Subsection 4.2.

5. RESULTS

First we test our algorithm on simulated data generated using the dipole equation (1) with additive white Gaussian noise of variance 6.25×10^{-2}, a magnet with $\frac{\mu_0 m}{4\pi} = 4 \times 10^{-4}\,\mathrm{J/\mu T}$, and a magnetometer of sampling frequency $f_s = 40\,\mathrm{Hz}$. We use three cases: 1) $r = 3\,\mathrm{cm}$, $v = 30\,\mathrm{cm/s}$, 2) $r = 3\,\mathrm{cm}$, $v = 60\,\mathrm{cm/s}$, 3) $r = 6\,\mathrm{cm}$, $v = 30\,\mathrm{cm/s}$. For each scenario we vary the directions $\mathbf{d}_r$, $\mathbf{d}_v$, and $\mathbf{d}_m$ to produce 10000 gestures.

For the algorithm, τ and ϕ are uniformly sampled respectively from 1 to 30 with a step of 1 and from 0 to 90° with a step of 0.5°. The results are summarized in Table 1 which shows very good detection, localization, and estimation abilities. $(\mathbf{d}, \hat{\mathbf{d}})$ denotes the angle between the direction $\mathbf{d}$ and the estimated direction $\hat{\mathbf{d}}$. $|\ell - \hat{\ell}|$ is the time index shift between the time and estimated time of a gesture detection.

Errors	$\lvert\ell - \hat{\ell}\rvert$	$\frac{\lvert r - \hat{r}\rvert}{r}$	$(\mathbf{d}_r, \hat{\mathbf{d}}_\mathbf{r})$	$\frac{\lvert v - \hat{v}\rvert}{v}$	$(\mathbf{d}_v, \hat{\mathbf{d}}_\mathbf{v})$	$\lvert\phi - \hat{\phi}\rvert$
Case 1	0	0.010	2.2°	0.019	0.8°	1.1°
Case 2	0	0.008	2.4°	0.012	1.2°	1.3°
Case 3	0.04	0.038	11.2°	0.118	5.2°	9.1°

Table 1. Average errors for 10000 simulated gestures

The algorithm is also tested on an iPhone 5 with iOS7, which embed a AK8975 [11] magnetometer ($f_s = 40\mathrm{Hz}$). We use an Apple earphone (with $\frac{\mu_0 m}{4\pi} = 4 \times 10^{-4}\,\mathrm{J/\mu T}$) as magnet. Figure 2 shows a typical observed signal and its estimate. The algorithm demonstrates promising results even for tracking movements performed by a human.

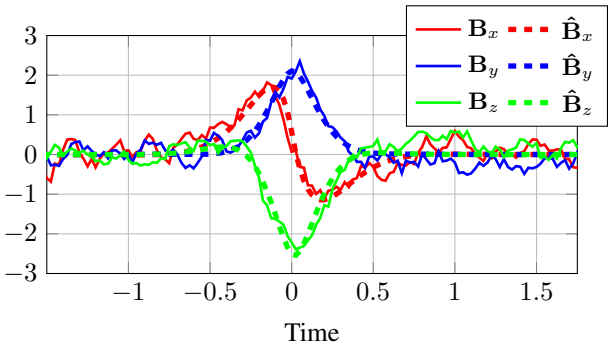

Fig. 2. Raw measurements and estimated signals

6. CONCLUSION

We have modeled magnetic field variations produced by a moving magnet with a bank of 6^{th}-order linear state space models. Each model accounts for a specific time-scale. The information on the gesture is contained in the observation matrix, which is restricted to a specific set. Due to nice recursions for computing the localized squared error and the ability to get a fast approximation of the minimum cost, this simple model is suitable for a robust and efficient detection and estimation of uniform straight-line movements performed with a magnet. This algorithm has the convenient property to run in real-time on modern mobile devices.

7. REFERENCES

[1] H. Ketabdar, M. Roshandel, and K. A. Yüksel, "Towards using embedded magnetic field sensor for around mobile device 3d interaction," in *Proceedings of the 12th international conference on Human computer interaction with mobile devices and services*. ACM, 2010, pp. 153–156.

[2] M. Birsan, "Unscented particle filter for tracking a magnetic dipole target," in *OCEANS MTS/IEEE Proceedings*, 2005, pp. 1656–1659.

[3] M. Birsan, "Recursive bayesian method for magnetic dipole tracking with a tensor gradiometer," *IEEE Transactions on Magnetics*, vol. 47, no. 2, pp. 409–415, 2011.

[4] H. M. Schepers, D. Roetenberg, and P. H. Veltink, "Ambulatory human motion tracking by fusion of inertial and magnetic sensing with adaptive actuation," *Medical & biological engineering & computing*, vol. 48, no. 1, pp. 27–37, 2010.

[5] N. Wahlstrom, J. Callmer, and F. Gustafsson, "Single target tracking using vector magnetometers," in *IEEE International Conference on Acoustics, Speech and Signal Processing (ICASSP)*, 2011, pp. 4332–4335.

[6] N. Wahlstrom, R. Hostettler, F. Gustafsson, and W. Birk, "Rapid classification of vehicle heading direction with two-axis magnetometer," in *IEEE International Conference on Acoustics, Speech and Signal Processing (ICASSP)*, 2012, pp. 3385–3388.

[7] N. Wahlstrom and F. Gustafsson, "Magnetometer modeling and validation for tracking metallic targets," *IEEE Transactions on Signal Processing*, vol. 62, no. 3, pp. 545–556, 2014.

[8] R. Otnes, "Static magnetic dipole detection using vector linear prediction, anderson functions, and block-based adaptive processing," in *OCEANS - Europe*, 2007, pp. 1–6.

[9] L. Bruderer, H.-A. Loeliger, and N. Zalmai, "Local statistical models from deterministic state space models, likelihood filtering, and local typicality," in *IEEE International Symposium on Information Theory (ISIT)*, 2014, pp. 1106–1110.

[10] P. H. Schönemann, "A generalized solution of the orthogonal procrustes problem," *Psychometrika*, vol. 31, no. 1, pp. 1–10, 1966.

[11] "Specifications of the compass sensor AK8975," `http://www.akm.com/akm/en/file/datasheet/AK8975.pdf`, Accessed: 2014-09-15.